

FATIGUE CRACKS AT RUNWAYS OF MONORAIL GIRDERS

By Ichiro OKURA*, Kiyoshi HORIIKE** and Yuhshi FUKUMOTO***

Fatigue cracks at runways of steel track girders for a straddle type monorail have been studied experimentally and analytically. Full-scale fatigue tests of runways showed that repeated plate-bending stresses caused fatigue cracks at single-bevel groove-welded T-joints between top flange and web and also at fillet welds connecting the longitudinal rib to the top flange. For fatigue lives over ten million cycles, fatigue strengths of single-bevel groove-welded T-joints under out-of-plane bending were obtained using small specimens. Equations for plate-bending stresses were given by a parametric study by F. E. M. Minimum thicknesses required for the top flange to prevent cracking were proposed.

Keywords: fatigue, monorail girder, runway

1. INTRODUCTION

Steel track girders for the Osaka Monorail are now under construction at the section of 13.7 km from the Osaka International Airport to the Minami-Ibaragi Station on Osaka-to-Kyoto line of Hankyu-Railway. The Osaka Monorail is of a straddle type. Prestressed concrete girders with a span length of 22 m are usually used. Steel track girders are, however, constructed at the intersections with existing roads, crossings above rivers and sections with complicated curved lines. As shown in Fig. 1, they are narrow box girders with 660 mm in width and 2.2 m to 3.3 m in height. Parallel track girders are connected with cross beams of I-section. Wheels of monorail cars run on the top flange of the girders.

The runways of steel track girders are designed according to the provisions for orthotropic steel decks in the Japanese highway and railway bridge specifications^(1,2). In design of orthotropic steel decks, generally the following items have to be considered:

- (a) To work as a part of main girders.
- (b) To work as a floor system consisting of longitudinal and transverse ribs.
- (c) To work as a floor slab supporting directly wheel loads.

Stress check is imposed for the items (a) and (b) in the highway and railway bridge specifications. On the contrary, the commentary in the highway bridge specification says that we do not need to consider the item (c) if the thickness of a deck plate is not less than the value calculated by the following equation:

$$t = 0.035 b, \text{ but } t \geq 12 \text{ mm} \dots \dots \dots (1)$$

* Member of JSCE, Dr. Eng., Assistant Professor, Department of Civil Engineering, Osaka University (Yamadaoka 2-1, Suita, Osaka 565)

** Member of JSCE, M. Eng., Sumitomo Metal Industries, Ltd., formerly Graduate Student, Department of Civil Engineering, Osaka University

*** Member of JSCE, Ph. D., Dr. Eng., Professor, Department of Civil Engineering, Osaka University

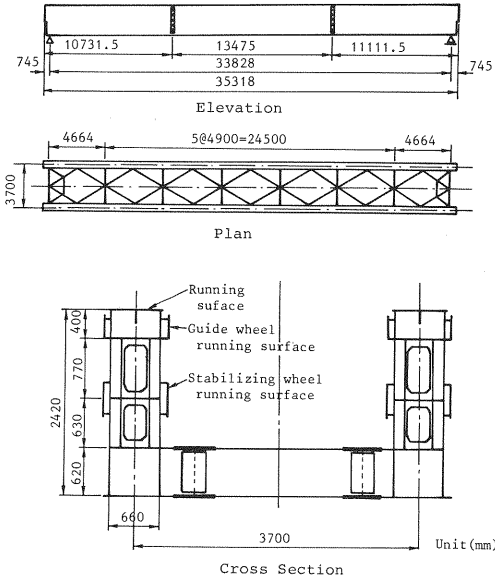


Fig. 1 General view of steel track girders.

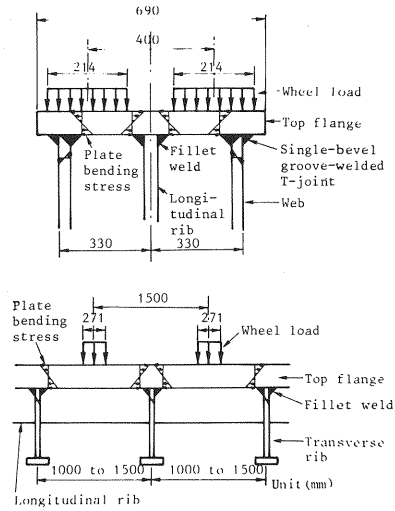


Fig. 2 Plate-bending stresses on runway.

where t =minimum thickness of a deck plate. (mm)
 b =interval between longitudinal ribs. (mm)

Also, in the railway bridge specification, we do not need to pay attention to the item (c), if the thickness of a deck plate is not less than 12 mm and the interval between longitudinal ribs is not greater than 30 times of the thickness of a deck plate.

In straddle type monorails, as shown in Fig. 2, plate-bending stresses occur at the toes on the top flange side and on the web side of the single-bevel groove-welded T-joint connecting the web to the top flange, because wheel loads run on the top flange in eccentricity about the web plate. Similarly, they are initiated at the toes on the top flange side of the fillet welds to connect the longitudinal rib to the top flange. Besides, they occur at the toes on the top flange side and on the transverse rib side of the fillet welds to connect the transverse rib to the top flange. As will be mentioned in Chapter 2, those plate-bending stresses are produced every time when each axle of monorail cars passes on adjacent transverse ribs. There will be a possibility of cracking in operation because of a large number of cycles of load. It is doubtful whether the thickness of 12 mm for the top flange given by the highway and railway bridge specifications is enough to keep the plate-bending stresses low and to prevent cracking.

The object of this investigation is to obtain the minimum thicknesses required for the top flange to prevent cracking due to plate-bending stresses.

2. STRESS ANALYSIS OF RUNWAY

(1) Analytical model

A finite element analysis was carried out for such a model as shown in Fig. 3. A transverse rib is provided in the middle. The top flange, web and longitudinal rib are 18 mm, 10 mm and 16 mm thick, respectively. The condition of symmetry was imposed at the location of the longitudinal rib, because the structure of the runway is symmetrical about the longitudinal rib and wheel loads are also applied symmetrically about the longitudinal rib. The cross-sectional deformation was fixed at both the ends of the analytical model. Besides, the displacement in the vertical direction at the bottom edge of the web was fixed. Wheel loads were applied uniformly on the rectangular region of 271 mm×214 mm in the middle of the left panel, which has the same area as the contact area of a tire of monorail cars. In the finite element

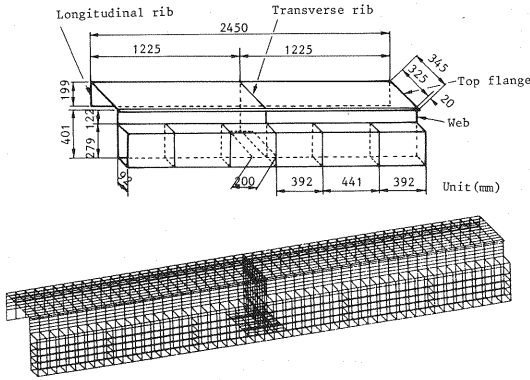


Fig. 3 Analytical model of runway.

analysis, rectangular plate elements with 6 degrees at each node were used³⁾.

(2) Analytical results

The distribution of the plate-bending stresses under wheel loads is shown in Fig. 4. The plate-bending stresses on the outer surfaces of the top flange and web are given in the figure. The weight of one wheel is 44 kN, which is half the weight of one axle in the fatigue design⁴⁾. The plate-bending stresses are not produced on the longitudinal rib from the characteristic of symmetry. Large plate-bending stresses occur on the top flange at the location of the longitudinal rib and at the top edge of the web. A membrane stress also occurs on the web. Its magnitude is -8.7 MPa at the top edge of the web, which is about 10 % of the plate-bending stress.

The distributions in the longitudinal direction of the plate-bending stresses on the top flange at the location of the longitudinal rib and at the top edge of the web are shown in Fig. 5. Each of the plate-bending stresses takes a maximum value in the middle of the left panel on which wheel loads are applied, while it is almost zero on the right panel. The minimum interval of axles of monorail cars is 1 500 mm⁴⁾. When transverse ribs are provided at an interval less than 1 500 mm, each axle produces independently plate-bending stresses on the top flange and web between adjacent transverse ribs. In steel track girders for the Osaka Monorail, the transverse ribs in the runways are provided at an interval between 1 000 mm and 1 500 mm because of the design for the item (b) mentioned in Chapter 1. The number of trains which pass on one track for a design life span of 70 years is 2.81×10^6 , and one train has 24 axles⁴⁾. Therefore, the fatigue design life for the runways becomes 6.75×10^7 cycles.

3. FULL-SCALE FATIGUE TESTS OF RUNWAYS

(1) Outline of fatigue tests

A fatigue test specimen is shown in Fig. 6. Transverse ribs are provided at both the ends and at one-third points between them. The dimensions of the specimen and the welding conditions are the same as those of actual structures⁵⁾. A Japanese SM50YB steel with the minimum specified yield and tensile strengths of 353 MPa and 490 MPa respectively, was used for the longitudinal rib, and SM41A and SM41B steels, which have both the minimum specified yield and tensile strengths of 235 MPa and 402 MPa, respectively, were used for the plates other than the longitudinal rib.

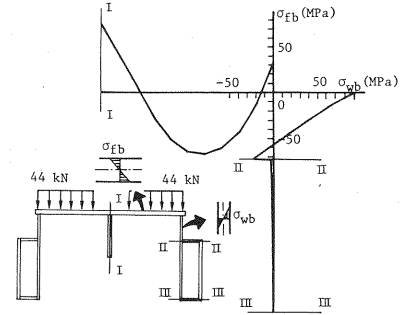
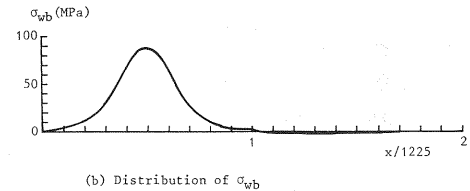
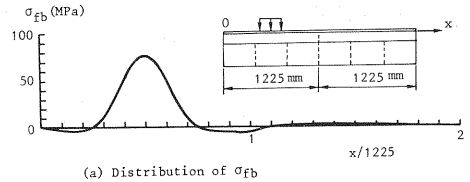


Fig. 4 Distribution of plate-bending stresses under wheel loads.

Fig. 5 Distributions in the longitudinal direction of σ_{fb} and σ_{wb} .

Loading cases are shown in Table 1. As shown in the figure inserted in the table, the load was applied on two rectangular regions of which centers are 400 mm apart. Six loading cases were considered for three test specimens. In Specimens 1 and 3, the load pulsator was applied in the middle between adjacent transverse ribs, while in Specimen 2, it was applied just on the transverse rib.

Fatigue tests were performed by a servo-type 1 000 kN capacity fatigue testing machine at the Chiba Research Center of Mitsui Engineering & Shipbuilding Co., Ltd. Overall view of the test setup is shown in Photo 1. The test specimen is laid on the top flange of a box-type supporting of 1 m in height. The bottom edge of the web of the specimen touches the top flange of the supporting. A rubber plate 30 mm thick was inserted between the loading table and the top flange of the test specimen.


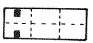
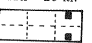
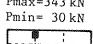

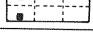
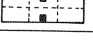
(2) Test results of specimens 1 and 3

Fatigue cracks were observed at the toe on the web side of the single-bevel groove-welded T-joint between top flange and web (Type A fatigue crack) and also at the toe on the top flange side of the fillet weld connecting the longitudinal rib to the top flange (Type B fatigue crack). They were initiated at the locations where the F.E.M. analysis had shown large plate-bending stresses, in the middle between adjacent transverse ribs.

Type A fatigue cracks were initiated at Loading Cases (1, 1), (1, 2), (1, 3) and (3, 1). The fatigue fracture surface is shown in Photo 2. The bright part is the brittle fracture surface by a destructive testing. A crack starts from the outside surface of the web, propagates across the web thickness and stops about 2 mm from the inside surface. Another crack occurs from the inside surface of the web. The fatigue cracks from the outside and inside surfaces are initiated on the tension and compression sides of the plate-bending stress, respectively.

Type B fatigue cracks were detected in Loading Case (1, 1) and (1, 2). Photo 3 shows a crack which occurred at the toe of the fillet weld on the right side. It propagates by about half across the thickness of

Table 1 Loading cases.

Specimen	Loading cases		
	1	2	3
1	Pmax=265 kN Pmin= 35 kN 	Pmax=304 kN Pmin= 48 kN 	Pmax=373 kN Pmin= 20 kN 
2	Pmax=343 kN Pmin= 30 kN 	 Unit (mm)	
3	Pmax=265 kN Pmin= 32 kN 	Pmax=196 kN Pmin= 28 kN 	

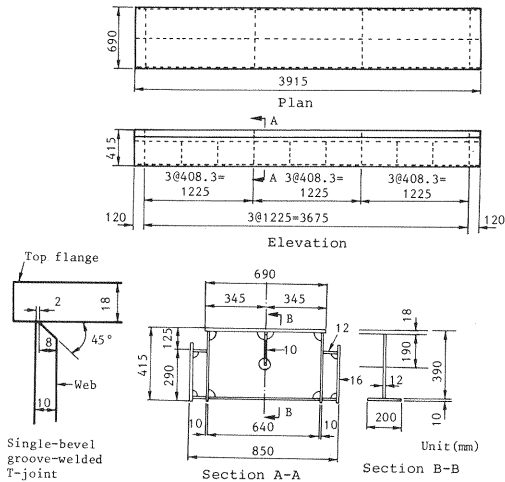


Fig.6 Full-scale fatigue test specimen.

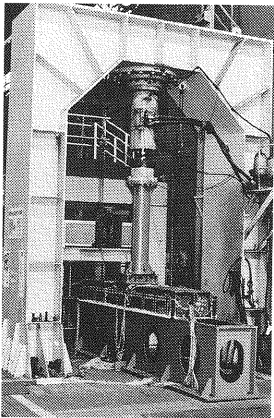


Photo 1 Fatigue test of runway.

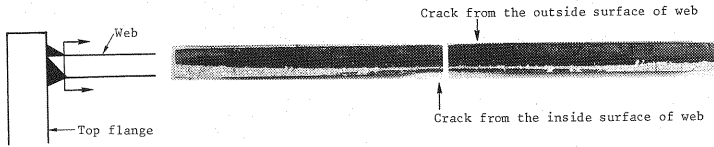


Photo 2 Fracture surface of Type A fatigue crack.

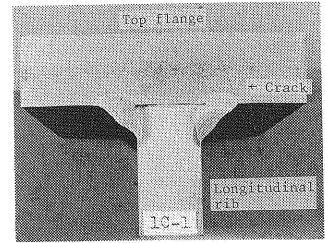


Photo 3 Type B fatigue crack.

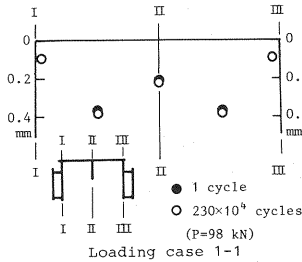


Fig. 7 Out-of-plane deflection of top flange.

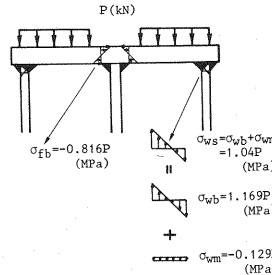


Fig. 8 Relations between surface stress and axle load.

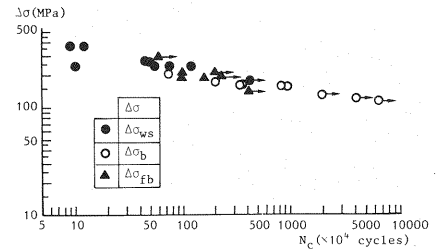


Fig. 9 S-N relation.

the top flange. It occurs at the compression side of the plate-bending stress.

The distribution of out-of-plane deflection of the top flange at the termination of the fatigue test is shown in Fig. 7. The amount of the out-of-plane deflection changes little in spite of the crack propagation.

(3) Test results of specimen 2

Fatigue cracks were not detected at 2.04×10^6 cycles. The strain gauges which were mounted nearby the stress concentration points did not show such strains as to cause fatigue cracks even when the load was increased to 373 kN.

(4) S-N relation

The range of surface stress at the weld toe was used for S in the S-N relation. The relations between surface stress and axle load are shown in Fig. 8. They were obtained by extrapolation of the measured stresses nearby the crack initiation⁶⁾. The membrane stress on the top flange was almost zero. Using the relations in Fig. 8, stress ranges $\Delta\sigma_{ws}$ and $\Delta\sigma_{fb}$ were calculated for Types A and B fatigue cracks, respectively.

N_c in the S-N relation was defined as the number of cycles when a crack grew by 20 mm along the weld toe. Dye-penetrant inspection was used to detect surface cracks. Fig. 9 shows the relation between $\Delta\sigma_{ws}$ or $\Delta\sigma_{fb}$ and N_c . In the figure, black circles and triangles correspond to $\Delta\sigma_{ws}$ and $\Delta\sigma_{fb}$, respectively.

4. FATIGUE TESTS OF SMALL SPECIMENS

(1) Outline of fatigue tests

Fatigue tests of single-bevel groove-welded T-joints subjected to out-of-plane bending were carried out over ten million cycles. A test specimen is shown in Fig. 10. The vertical and horizontal plates are of SM41B and SM41A steels, respectively. They are connected by single-bevel-groove-welds. The fatigue tests were performed by a servo-type 200 kN capacity fatigue testing machine at the Department of Civil Engineering of Osaka University. Overall view of the test setup is shown in Photo 4. The plate-bending stress in tension is caused at the weld toe on the bottom surface of the horizontal plate.

(2) Test results

Table 2 shows test results. In the table, N_c is the number of cycles when a crack grew by 20 mm along the weld toe, and N_f is the number of cycles when a test specimen broke. In Specimen 6, fatigue cracks were not observed for early three load ranges at about twenty million cycles.

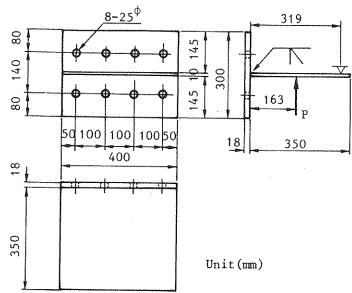


Fig. 10 Small specimen.

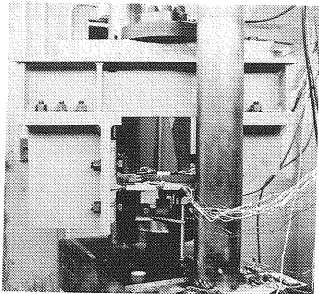


Photo 4 Fatigue test of small specimen.

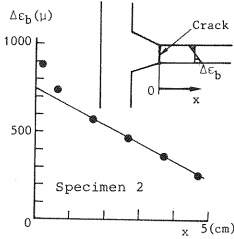
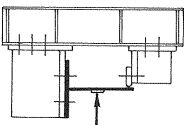


Fig. 11 Distribution of plate-bending strain range.

The way to determine the values of $\Delta\sigma_b$ in Table 2 is as follows : Fig. 11 shows the distribution of the plate-bending strain in the direction perpendicular to the weld line. In the figure, the distance from the weld toe is taken on the longitudinal axis. The range of plate-bending strain increases in the very vicinity of the weld toe due to the stress concentration at the weld toe. The distribution of strain range shows a straight line far from the weld toe. The strain value at the weld toe by extrapolation of that straight line was converted into the stress range by the following equation :

$$\Delta\sigma_b = E\Delta\epsilon_b / (1 - \nu^2) \dots \dots \dots (2)$$

where $\Delta\sigma_b$ = plate-bending stress range at the weld toe.
 $\Delta\epsilon_b$ = plate-bending strain range at the weld toe.
 E = Young's modulus.
 ν = Poisson's ratio.

The relation between $\Delta\sigma_b$ and N_c is expressed by white circles in Fig. 9.

5. EQUATIONS FOR PLATE-BENDING STRESSES

(1) Analytical model

Equations for plate-bending stresses at the single-bevel groove-welded T-joint connecting the web to the top flange and at the fillet weld connecting the longitudinal rib to the top flange were obtained by a parametric study by F. E. M. The analytical model is shown in Fig. 12. It is composed of the cross section expressed by thick lines in the inserted figure in Fig. 12 and of the part between adjacent transverse ribs. The boundary conditions at the bottom edge of the web are shown in Fig. 13. The plate-bending stresses at the single-bevel groove-welded T-joint and at the fillet weld were calculated under the boundary conditions (I) and (III), respectively, because they showed the largest value for those boundary conditions, respectively.

(2) Analytical results

The width of the top flange and the height of the web are specified from the clearance limit for monorail cars. The thickness of the top flange (t_f), the thickness of the web (t_w), the width and thickness of

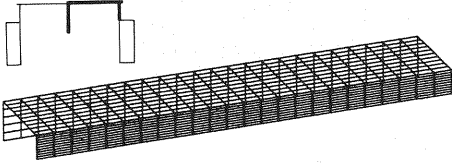


Fig. 12 F.E.M. model for parametric analysis.

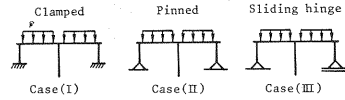


Fig. 13 Boundary conditions at the bottom edge of the web.

longitudinal rib (h_r , t_r) and the interval between adjacent transverse ribs (L) have to be determined by designers. In steel track girders for the Osaka Monorail, longitudinal ribs with 190 mm in width and 16 mm to 19 mm in thickness are used because of the design for the item (b) mentioned in Chapter 1. In the parametric analysis, the following ranges were considered for those parameters :

$$12 \text{ mm} \leq t_f \leq 37 \text{ mm}, \quad 8 \text{ mm} \leq t_w \leq 12 \text{ mm}, \quad 16 \text{ mm} \leq t_r \leq 19 \text{ mm}, \quad 1000 \text{ mm} \leq L \leq 1500 \text{ mm}, \quad h_r = 190 \text{ mm}$$

A curve fitting technique to the results by F.E.M. gave the following equations^{(6),(7)} :

$$\sigma_{wb} = 5.058 \times 10^3 \times 10^{-0.173 t_w} \times t_f^{(-2.89 + 0.137 t_w)} \times P \dots\dots\dots (3)$$

$$\sigma_{fb} = -(3.902 \times 10^2 \times t_f^{-1.87} - 1.284 \times 10^{-2} \times t_f^{-1.02} \times L) \times P \dots\dots\dots (4)$$

where σ_{wb} and σ_{fb} = plate-bending stresses at the single-bevel groove-welded T-joint connecting the web to the top flange and at the fillet weld connecting the longitudinal rib to the top flange, respectively. (MPa)

P = axle load. (kN)

A comparison of the estimated values from Eqs. (3) and (4) with the F.E.M. values is shown in Fig. 14. The estimated values approximate the F.E.M. values very well.

(3) Plate-bending stresses at weld toe

As shown in Fig. 15, Eqs. (3) and (4) give the plate-bending stress at the intersection of the middle planes of each plate. To represent the plate-bending stresses at the weld toes, these equations were modified by the following way :

An L-shaped frame is shown in Fig. 16 (a). The shape of the frame is the same as that of the cross section of the analytical model in Fig. 12 except the part of the longitudinal rib. The frame is 10 mm wide. In this analytical model, the welding shape of the single-bevel groove-welded T-joint between web and top flange and also the welding shape of the fillet weld between longitudinal rib and top flange are considered. The average value of the welding legs measured on the full-scale fatigue test specimens was used in the model. A concentrated load was applied at the center of the beam of the L-shaped frame. The right end of the beam and the bottom end of the column were both fixed. Calculations were performed for plane stress conditions by F.E.M. with two-dimensional 8-node isoparametric elements⁽⁹⁾. On the other hand, an L-shaped frame shown in Fig. 16(b) was solved by the beam theory. In this model, the welding shape is not considered.

An example of comparisons of the plate-bending stresses obtained from F.E.M. and Beam models with the flange 18 mm thick and web 10 mm thick is shown in Fig. 17. The magnitude of the load P is 981 N. It is seen from Fig. 17 that the distributions of plate-bending stresses by F.E.M. and Beam models are quite

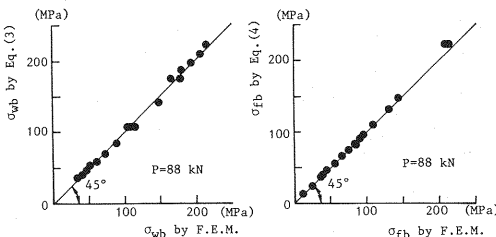


Fig. 14 Comparison of estimated values with F.E.M. values.

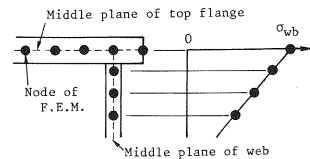


Fig. 15 Plate-bending stress given by plate element.

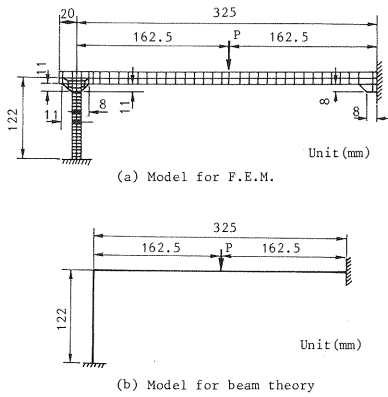


Fig. 16 L-shaped frame.

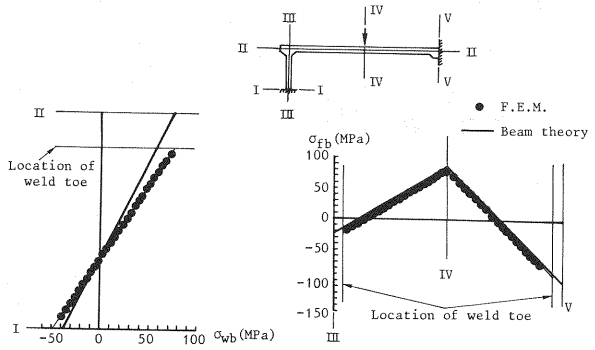


Fig. 17 Comparison of plate-bending stresses.

Table 3 Comparison of plate-bending stresses.

t_w (mm) (1)	t_f (mm) (2)	$\sigma_{wb}(F.E.M.)$ (MPa) (3)	$\sigma_{wb}(beam)$ (MPa) (4)	$-\sigma_{fb}(F.E.M.)$ (MPa) (5)	$-\sigma_{fb}(beam)$ (MPa) (6)	r_w {(3)/(4)} (7)	r_f {(5)/(6)} (8)
8	12	162.6	164.8	191.6	212.4	0.987	0.902
8	18	75.9	70.8	91.5	103.7	1.072	0.882
8	31	17.8	16.4	32.0	36.8	1.085	0.870
10	12	134.8	144.9	180.1	198.7	0.930	0.906
10	18	74.5	74.9	87.1	99.1	0.995	0.879
10	31	20.9	19.6	31.4	36.3	1.066	0.865
12	12	109.0	120.7	171.0	188.7	0.903	0.906
12	18	68.6	73.3	83.1	94.4	0.936	0.880
12	31	22.7	22.3	30.7	35.6	1.018	0.862

$\sigma_{wb}(F.E.M.)$ = plate-bending stress at the toe on the web side of the single-bevel groove-welded T-joint in F.E.M. model.
 $\sigma_{fb}(F.E.M.)$ = plate-bending stress at the toe on the flange side of the fillet weld in F.E.M. model.
 $\sigma_{wb}(beam)$ = plate-bending stress on the web side at the intersection of the neutral axes of beam and column in Beam model.
 $\sigma_{fb}(beam)$ = plate-bending stress at the right end of the beam in Beam model.

different on the column.

The comparison of the plate-bending stresses at the weld toes is listed in Table 3. $\sigma_{wb}(F.E.M.)$ and $\sigma_{fb}(F.E.M.)$ were obtained by extrapolation of the distributions of F. E. M. results in Fig. 17. r_w and r_f in Table 3 are defined as follows :

$$r_w = \sigma_{wb}(F.E.M.) / \sigma_{wb}(beam) \dots \dots \dots (5)$$

$$r_f = \sigma_{fb}(F.E.M.) / \sigma_{fb}(beam) \dots \dots \dots (6)$$

By applying the least squares method to the r_w values of the column (7) in Table 3, r_w was formulated as follows :

$$r_w = -0.0243 t_w + 0.0059 t_f + 1.122 \dots \dots \dots (7)$$

Equation (7) approximates the values of the column (7) in Table 3 with relative errors within 4 %.

Using r_w , Eq. (3) was modified as follows to give the plate-bending stress at the weld toe :

$$\sigma_{wb} = 5.058 \times 10^3 \times r_w \times 10^{-0.173 t_w} \times t_f^{(-2.89 + 0.137 t_w)} \times P \dots \dots \dots (8)$$

The figure 5.058 in Eq. (8) was then replaced by 5.062 so that Eq. (8) could take the same σ_{wb} value as given in Fig. 8 which was obtained from the full-scale fatigue tests. Equation (3) was finally modified as follows :

$$\sigma_{wb} = 5.062 \times 10^3 \times (-0.0243 t_w + 0.0059 t_f + 1.122) \times 10^{-0.173 t_w} \times t_f^{(-2.89 + 0.137 t_w)} \times P \dots \dots \dots (9)$$

As for r_f , it is not necessary to make an equation like r_w , because as can be seen from the column (8) in Table 3, r_f does not show large variation. To adjust Eq. (4) to the σ_{fb} value in Fig. 8, Eq. (4) was multiplied by 0.891, resulting in the following equation :

$$\sigma_{fb} = -(3.477 \times 10^2 \times t_f^{-1.87} - 1.144 \times 10^{-2} \times t_f^{-1.02} \times L) \times P \dots \dots \dots (10)$$

6. MINIMUM THICKNESSES OF TOP FLANGE

The condition to prevent Type A fatigue cracks is as follows :

$\sigma_{wb} + \sigma_{wm} \leq \sigma_{fatigue}$ (11)
 where σ_{wm} = membrane stress at the toe of the single-bevel groove-welded T-joint connecting the web to the top flange.

$\sigma_{fatigue}$ = fatigue strength at the design cycles of 6.75×10^7 .

In Fig. 9, we cannot estimate the fatigue strength at 6.75×10^7 cycles by the statistical procedure because of the shortage of the test results for fatigue lives over ten million cycles. Then, 150 MPa was used for $\sigma_{fatigue}$, based on the following facts :

- (a) No fatigue cracks occurred at the stress range less than 150 MPa in Fig. 9.
- (b) As seen from the comparison of σ_{wb} with σ_{wm} in Fig. 8, σ_{wm} is about 10 % of σ_{wb} and compressive. Neglecting σ_{wm} from Eq. (11), we can estimate Type A fatigue cracks on the conservative side.
- (c) Even when Type A fatigue cracks are initiated, the serviceability of the runway is preserved, because the out-of-plane deflection of the top flange changes little after the propagation of Type A fatigue cracks, as was shown in Fig. 7.

Neglecting σ_{wm} from Eq. (11), substituting 150 MPa for $\sigma_{fatigue}$, and considering Eq. (9), the following equation was obtained as the condition to prevent Type A fatigue cracks :

$$5.062 \times 10^3 \times (-0.0243 t_w + 0.0059 t_f + 1.122) \times 10^{-0.173 t_w} \times t_f^{(-2.89 + 0.137 t_w)} \times P \times (1 + i) \leq 150 \text{ (12)}$$

The axle load P and impact factor i in the fatigue design of the runways of steel track girders for the Osaka Monorail are 88 kN and 0.5, respectively⁴⁾. From Eq. (12), the following minimum thicknesses were obtained for the top flange :

$t_f = 19 \text{ mm}$ for $t_w = 8, 9, 10 \text{ mm}$

$t_f = 18 \text{ mm}$ for $t_w = 11, 12 \text{ mm}$

In the top flanges with these thicknesses, the plate-bending stress estimated by Eq. (10) for Type B fatigue cracks does not exceed 125.7 MPa. From Fig. 9, Type B fatigue cracks will not occur at the plate-bending stress range of 125.7 MPa for the design cycles of 6.75×10^7 .

7. CONCLUSIONS

The fatigue cracks due to plate-bending stresses at the runways of steel track girders for a straddle type monorail were studied experimentally and analytically. The main results are as follows :

- (1) Full-scale fatigue tests of runways showed that repeated plate-bending stresses caused fatigue cracks at the single-bevel groove-welded T-joints between top flange and web and also at the fillet welds connecting the longitudinal rib to the top flange.
- (2) For fatigue lives over ten million cycles, fatigue strengths of single-bevel groove-welded T-joints under out-of-plane bending were obtained using small specimens.
- (3) Equations for plate-bending stresses were given by a parametric study by F. E. M.
- (4) Minimum thicknesses required for the top flange to prevent cracking were proposed.

ACKNOWLEDGMENTS

We would like to thank Prof. Y. Maeda, Kinki University, for his valuable comments on this paper. We would also like to thank Messrs. I. Konishi, Y. Ogasawara and K. Isozaki, Osaka Prefectural Government, and Messrs. Y. Iwai and T. Fukuoka and M. Sawayanagi, Mitsui Engineering & Shipbuilding Co., Ltd. for their help in carrying out the fatigue tests.

REFERENCES

- 1) Japan Road Association : Specifications for Highway Bridges, Part II, 1980. (in Japanese)
- 2) JSCE : Specifications for Steel Railway Bridges, 1983. (in Japanese)
- 3) Zienkiewicz, O. C. and Cheung, Y. K. : The Finite Element Method in Structural and Continuum Mechanics, McGraw-Hill, pp. 66-67, pp. 90-98 and pp. 124-137, 1967.
- 4) Civil Engineering Bureau of Osaka Prefectural Government : Specification for Structures of Osaka Monorail, 1982. (in

Japanese)

- 5) Osaka Prefectural Government and Mitsui Engineering & Shipbuilding Co., Ltd. : Fatigue Tests of Runways of Steel Track Girders for Osaka Monorail, March, 1986. (in Japanese)
- 6) Okura, I., Horiike, K. and Fukumoto, Y. : Fatigue cracks at runway of steel track girders for straddle type monorails, Journal of Structural Engineering, Vol.34A, JSCE, pp.513-524, 1988. (in Japanese)
- 7) Horiike, K. : Fatigue strength of runway of steel track girders for straddle type monorails, M.E. Thesis, Osaka University, 1987.
- 8) Zienkiewicz, O.C. : The Finite Element Method, McGraw-Hill, pp.178-210, 1977.

(Received September 19 1988)
